

Collapse of the Normal State Pseudogap at a Lifshitz Transition in $\text{Bi}_2\text{Sr}_2\text{CaCu}_2\text{O}_{8+\delta}$ Cuprate Superconductor

S. Benhabib¹, A. Sacuto¹, M. Civelli², I. Paul¹, M. Cazayous¹, Y. Gallais¹, M.-A. Méasson¹, R. D. Zhong³, J. Schneeloch³ and G. D. Gu³, D. Colson⁴ and A. Forget⁴

¹ *Laboratoire Matériaux et Phénomènes Quantiques (UMR 7162 CNRS),*

Université Paris Diderot-Paris 7, Bat. Condorcet, 75205 Paris Cedex 13, France,

² *Laboratoire de Physique des Solides, (UMR 8502 CNRS),*

Université Paris Sud, Bat.510, 91405 Orsay Cedex,

³ *Matter Physics and Materials Science, Brookhaven National Laboratory (BNL), Upton, NY 11973, USA,*

⁴ *Service de Physique de l'Etat Condensé, CEA-Saclay, 91191 Gif-sur-Yvette, France*

(Dated: September 26, 2018)

We report a fine tuned doping study of strongly overdoped $\text{Bi}_2\text{Sr}_2\text{CaCu}_2\text{O}_{8+\delta}$ single crystals using electronic Raman scattering. Combined with theoretical calculations, we show that the doping, at which the normal state pseudogap closes, coincides with a Lifshitz quantum phase transition where the active hole-like Fermi surface becomes electron-like. This conclusion suggests that the microscopic cause of the pseudogap is sensitive to the Fermi surface topology. Furthermore, we find that the superconducting transition temperature is unaffected by this transition, demonstrating that their origins are different on the overdoped side.

PACS numbers: 74.72.Gh, 74.72.Kf, 74.25.nd, 74.62.Dh

Revealed more than twenty five years ago by nuclear magnetic resonance[1–3], the pseudogap phase in cuprates remains hitherto a mysterious state of matter out of which the high-temperature superconductivity emerges. The pseudogap appears below the T^* temperature and manifests itself as a loss of quasiparticle spectral weight. Although intensely studied in the underdoped regime [4–6], relatively less is known about the pseudogap on the overdoped side, where it weakens and eventually disappears. Thus, a logical line of enquiry is to study the pseudogap closing as a function of doping p , and to identify what triggers it in the first place.

In systems where $T^*(p)$ intersects the superconducting dome described by the critical temperature $T_c(p)$, this task is complicated by the appearance of the superconducting phase. One way to proceed is to perform such a study at the lowest available temperatures, either in the superconducting phase [7–12], or by suppressing it with magnetic field [13] or disorder[14]. Often such studies have inferred a quantum phase transition [15–17] associated with the pseudogap closing.

A second possibility is to track the *normal state* pseudogap at a higher temperature, and to study the vicinity of the doping p_c where it closes. Since p_c , defined as the doping where $T^*(p) = T_c(p)$, is essentially a finite temperature property, *a priori* it is not clear if it is linked to a quantum phase transition.

In this work our main result is to show that in $\text{Bi}_2\text{Sr}_2\text{CaCu}_2\text{O}_{8+\delta}$ (Bi-2212) p_c is indeed tied to a Lifshitz quantum phase transition where the underlying hole-like active Fermi surface becomes electron-like at a van Hove singularity. Interestingly, we find that T_c is unaffected by this transition. Moreover, comparing our results with existing photoemission and tunnelling data of several hole-doped cuprates, we infer that the microscopic origins of the pseudogap and the supercon-

ductivity are generically different on the overdoped side. Only the former is tied to the change in the Fermi surface topology, which removes quasiparticles from regions in momentum space of high scattering rate (hot regions). While the collapse of the normal state pseudogap [18–20], as well as the change of Fermi surface topology [21] have been reported earlier, to the best of our knowledge, the link between the two has not been demonstrated before in Bi-2212. Consequently, our result provides important clue regarding the microscopic origin of the normal state pseudogap, and its relation with superconductivity.

One technical obstacle to study pseudogap closing is the lack of sufficiently overdoped samples belonging to the same family of cuprates. Indeed, our study was made possible due to the availability of several high quality Bi-2212 single crystals with doping close to p_c , as reported in Supplemental Material (SM). The level of doping was controlled only by oxygen insertion, and the highest doping achieved was around $p = 0.24$. This allowed us to perform a careful finely tuned electronic Raman study of the doping dependence and determine $p_c = 0.22$.

The Raman measurements were performed in $\nu = B_{1g}, B_{2g}$ geometries that probe respectively the antinodal (AN) region near $(\pm\pi, 0)$ and $(0, \pm\pi)$ and the nodal (N) region near $(\pm\pi/2, \pm\pi/2)$, (cf. SM). Our spectra are comparable with earlier studies with a different laser line [22, 23], thereby demonstrating absence of resonance effects in the overall conclusions. In the following the quantity of importance is the integrated Raman intensity defined by

$$I_\nu(T) = \int_0^\Lambda d\omega \chi''_\nu(\omega, T), \quad (1)$$

extracted from the Raman response $\chi''_\nu(\omega, T)$ where Λ is a cutoff. We experimentally demonstrate our main result in two steps.

In the first step we determine p_c precisely, which is a refinement of our earlier work [18]. In Fig. 1, (a)-(d), we report Raman responses $\chi''_{B_{1g}}(\omega, T)$ at different temperatures and for different overdoped (OD) compounds. The temperature dependence of the corresponding integrated intensities $I_{B_{1g}}(T)$ are shown in Fig. 1.(e)-(h). In Fig. 1.a, we show the spectra for the Bi-2212 OD80 compound. We observe that the pair-breaking peak ($2\Delta_0$), located at 408 cm^{-1} , decreases in intensity with increasing temperature and disappears at T_c . Correspondingly, $I_{B_{1g}}(T)$ decreases monotonically exhibiting a dip at T_c (Fig.1.e). Just above T_c however, the low energy spectral weight (below 408 cm^{-1}) increases (positive slope) with temperature.

This recovery of spectral weight, which can be as large as 15% for $p = 0.11$ (cf. Fig. 3 in SM), is the signature of the presence of the pseudogap in the normal state spectra. Note that, this T -dependence is opposite to that of a normal metal. Therefore, above T_c , $I_{B_{1g}}(T)$ increases monotonically, until it reaches a maximum at a temper-

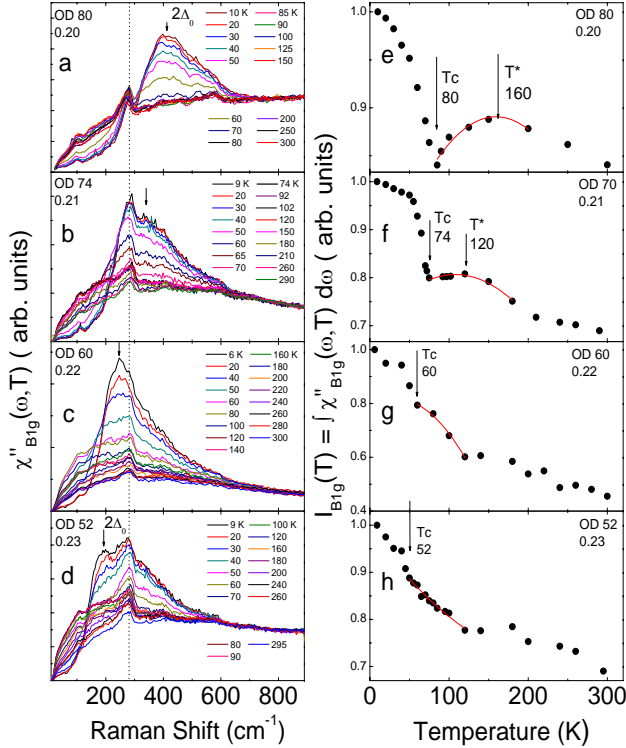


FIG. 1: (Color online)(a)-(d): T -dependence of the Raman response $\chi''_{B_{1g}}$ of overdoped Bi-2212. $2\Delta_0$ is defined as the position of the B_{1g} pair breaking peak. The location of the 300 cm^{-1} phonon peak is marked by a dotted line. (e)-(h): Integrated Raman intensities are shown in (a)-(d), with cut off $\Lambda = 850 \text{ cm}^{-1}$. For each doping, $I_{B_{1g}}(T)$ is normalized by $I_{B_{1g}}(10\text{K})$. The red curve is a second order polynomial fit just above T_c indicating the sign change of the slope. We found a remarkably linear dependence between T_c and $2\Delta_0$ in the critical temperature range $90 - 50 \text{ K}$ (cf. SM). The doping level for each value of T_c was fixed using the Tallon-Presland formula (cf.SM).

ature T^* that defines the onset temperature of the pseudogap (Fig.1.e). Above T^* , the T -dependence of $I_{B_{1g}}$ is the one of a normal metal. Our estimate of $T^*(p)$ is in good agreement with previous transport and spectroscopy measurements (cf. Fig. 4 of SM). As the doping level increases (Fig. 1. a-d), the difference between T_c and T^* shrinks, and disappears at $p_c = 0.22$, indicating the collapse of the normal state pseudogap. For $p > 0.22$ the slope of $I_{B_{1g}}(T)$ just above T_c is negative, implying there is no signature of the normal state pseudogap anymore. Quantitatively, this behavior is captured by the doping dependence of the loss of the spectral intensity, defined by $I_{B_{1g}}(T_c) - I_{B_{1g}}(T^*)$ and which we report in Fig. 3 as black stars. Note that a change in the slope of $I_{B_{1g}}(T)$ at $p \geq 0.22$ appears at $T \approx 100\text{K}$ which is definitely higher than the pseudogap $T^* \approx 60\text{K}$. Consequently, this feature is not related to the pseudogap, and its origin is currently under investigation.

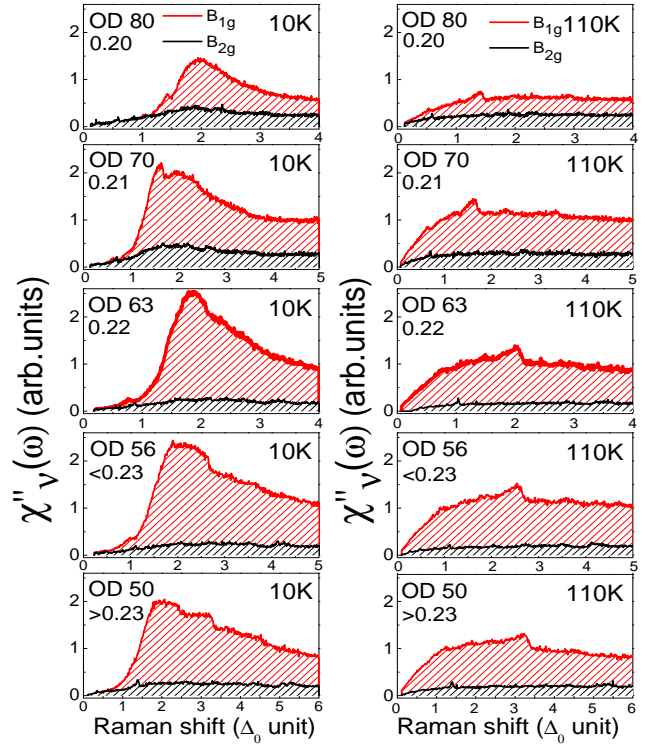


FIG. 2: (Color online) B_{1g} (red/grey) and B_{2g} (black) Raman responses of Bi-2212 at 10 K (superconducting state) and 110 K (normal state) in the overdoped range using 532 nm laser. The (red/grey) and black hatched areas indicate the magnitudes of the B_{1g} and the B_{2g} responses respectively. The former increases compared to the latter as a function of doping up to $p_c = 0.22$.

The second step involves comparing the spectra in the B_{1g} and B_{2g} geometries, and following their doping evolutions around p_c at fixed temperatures. Importantly, we succeeded in measuring the B_{1g} and B_{2g} Raman responses of each crystal on the same laser spot (see SM). We first show in Fig. 2 representative $\chi''_{B_{1g}}(\omega)$ (red/grey) and $\chi''_{B_{2g}}(\omega)$ (black) Raman responses, at 10 K (super-

conducting state) and at 110 K (normal state) for selected doping levels. The Raman shift is expressed in units of the superconducting gap $\Delta_0(p)$, in order to compare better samples with varying gap values. Note that, both in the superconducting and the normal states, the B_{1g} response increases continuously in magnitude compared to the B_{2g} response for $p \leq 0.22$, consistently with earlier studies [22, 24–30]. However, the crucial finding of the current work is that this trend changes and the B_{1g} response starts to decrease beyond 0.22 doping.

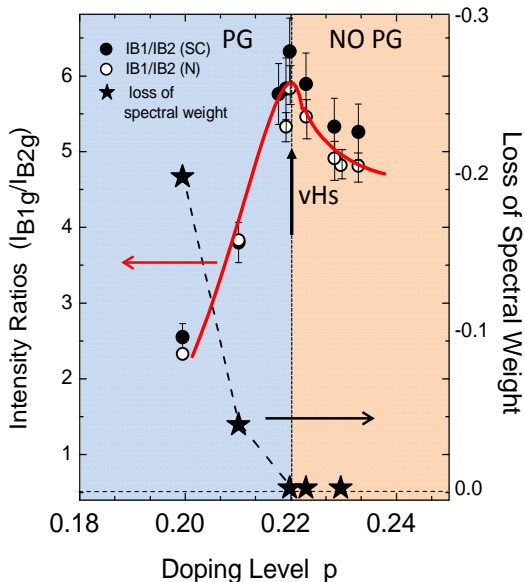


FIG. 3: (Color online) Doping evolution of (i) the ratio $I_{B_{1g}}/I_{B_{2g}}$ of the integrated intensity (defined in Eq. 1) in the superconducting and the normal states (filled and open circles respectively) with cutoff $\Lambda \approx 3\Delta_0$, (ii) the loss of spectral weight related to the pseudogap (black stars). The peak in the ratio $I_{B_{1g}}/I_{B_{2g}}$, both for the superconducting and the normal phases, coincides with the critical doping $p_c = 0.22$ where the pseudogap disappears. The peak is a consequence of a Lifshitz transition where the hole-like Fermi surface of the dominant anti-bonding band becomes electron-like as the chemical potential crosses a van Hove singularity.

The above non-monotonic doping dependence is best quantified by extracting the ratio of the integrated intensities $I_{B_{1g}}/I_{B_{2g}}$ from the Raman responses $\chi''_{\nu}(\omega)$ using Eq. 1. Studying the intensity ratio, rather than the absolute intensities, allow us to avoid spurious effects due to non intrinsic intensity modulations that may occur when passing from one crystal to another (cf.SM). Note that, in principle $I_{B_{1g}}$ contains not only the contribution of the electronic background (which is what we are interested in), but also that of the phonon peaked sharply at 300 cm^{-1} (see the dotted line in Fig. 1). However, by comparing the current spectra with that obtained using 647.1 nm laser line, in which the phonon peak is absent, we are able to confirm that $I_{B_{1g}}$, and especially its doping dependence, is mostly due to the electronic background [31].

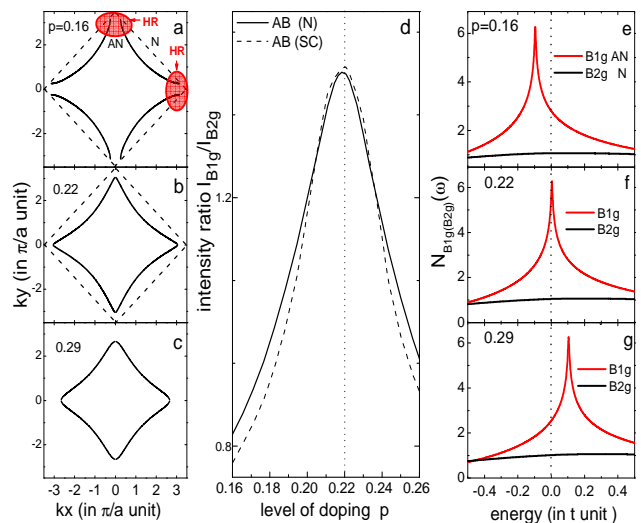


FIG. 4: (Color online) (a)-(c) With doping hole-like anti-bonding Fermi surface becomes electron-like at a Lifshitz transition. The dotted line is the antiferromagnetic Brillouin zone. HR denotes the hot region of large scattering rate. (d) Doping dependence of the integrated intensity ratio $I_{B_{1g}}/I_{B_{2g}}$ in the normal (solid line) and superconducting (dashed line) states calculated from a theoretical model (see text), reproducing qualitatively the trend of Fig. 3. The curves are normalized (cf.SM). (e)-(g). The associated van Hove singularity appears in $N_{B_{1g}}(\omega)$ (red/grey), the density of states weighted by the B_{1g} Raman vertex (defined in text), but not in $N_{B_{2g}}(\omega)$ (black), which is multiplied by $(t/t')^2$ for better visibility.

In Fig. 3 we report the doping dependencies of the intensity ratios $I_{B_{1g}}/I_{B_{2g}}$ in the superconducting (filled circles) and the normal states (open circles). Note that, the ratios in the two phases are nearly the same, thereby indicating that $I_{B_{1g}}/I_{B_{2g}}$ is unaffected by the superconducting gap. Most importantly, the ratios change non-monotonically as a function of p , and they reveal a sharp peak located at $p_c = 0.22$, the doping where the normal state pseudogap closes (black stars). We confirmed that the sharp peak is not a resonance effect, since it is visible with two distinct laser lines (532 nm and 647.1 nm).

Note that the peak in $I_{B_{1g}}/I_{B_{2g}}$ cannot be attributed to the doping dependence of the pseudogap which is monotonic. Instead, the temperature independence of the sharp peak position indicates that it is related to enhanced density of states of the underlying band structure around the AN region of the Brillouin zone. This invariably leads to the possibility of a doping induced Lifshitz transition wherein, as a van Hove singularity crosses the chemical potential, the open hole-like anti-bonding Fermi surface closes around the $(\pm\pi, 0)$ and $(0, \pm\pi)$ points and becomes electron-like. An electron-like anti-bonding band in Bi-2212 at $p > 0.22$ has been reported by ARPES data [21], but this change of topology was not linked with the closing of the pseudogap.

In order to support this scenario we perform theoretical calculation of the Raman response function using a minimal tight-binding model

with the normal state dispersion [32]: $\epsilon_{k,\alpha} = -2t(\cos k_x + \cos k_y) + 4t' \cos k_x \cos k_y \pm t_o(\cos k_x - \cos k_y)^2/4 - \mu$. Here $\alpha = \pm$ refer to the anti-bonding (AB) and the bonding (B) bands. The superconducting dispersion is

$E_k = \sqrt{\epsilon_k^2 + \Delta_k^2}$, with $\Delta_k = \Delta_0(\cos k_x - \cos k_y)/2$. We take $t' = -0.3t$, $t_o = 0.084t$, and a doping independent $\Delta_0 = 0.0025t$. We change p by varying the chemical potential μ . As shown in Fig. 4(a)-(c), this model undergoes a Lifshitz transition at $p_c = 0.22$ where the AB band changes from being hole- to electron-like (the B band remains hole-like in this doping range, see SM). For simplicity we take a constant electron scattering rate $\Gamma_N = 0.01t$ and $\Gamma_S = 0.0025t$ in the normal and the superconducting states respectively. An earlier work has shown that the scattering rates measured from the slopes of the Raman responses become isotropic around $p \approx 0.22$ [22]. The calculation of $\chi''_{\nu}(\omega)$ and I_{ν} are standard (for details, cf. SM). The doping dependence of the calculated ratio $I_{B_{1g}}/I_{B_{2g}}$ shows prominent peaks at $p = 0.22$ (see Fig. 4 (d)), both in the normal and the superconducting states, and reproduces qualitatively the experimental trend of Fig. 3.

The origin of the peak can be captured conveniently by tracking the doping dependence of the Raman vertex $\gamma_{k,\alpha}^{\nu}$ -weighted density of states $N_{\nu}(\omega) \equiv \sum_{k,\alpha} (\gamma_{k,\alpha}^{\nu})^2 \delta(\omega - \epsilon_{k,\alpha})$ which enter the calculation of I_{ν} . As shown in Fig. 4(e)-(g), the van Hove singularity shows up in $N_{B_{1g}}(\omega)$, and the peak in the intensity $I_{B_{1g}}$ corresponds to the van Hove singularity crossing the chemical potential. Simultaneously, since the B_{2g} geometry probes the diagonal directions of the Brillouin zone, $N_{B_{2g}}(\omega)$ is unaffected by the van Hove singularity and therefore $I_{B_{2g}}$ has no significant doping dependence.

Based on the Mott formula, at the Lifshitz transition $p = 0.22$ we expect a change in the sign of the Seebeck coefficient, provided the scattering rates are isotropic [33]. However, as noted in an earlier work [21], the Hall coefficient may remain positive across the Lifshitz transition, as observed in thin film studies [34].

A possible interpretation of our results is that the Lifshitz transition avoids the pseudogap by effectively moving quasiparticles from regions of strong scattering (hot regions) located around $(\pm\pi, 0)$ and $(0, \pm\pi)$ (see panels (a)-(c), Fig. 4). Note that, this possibility is independent of the origin of the hot regions which could arise from fluctuations of antiferromagnetic spin-waves [35–38] or charge-density waves (related to long-ranged incommensurate charge modulations)[39–44], or from Mott-related physics [45–49]. A second quantum critical point at p^* inside the superconducting dome, separating a small from a large FS phase, has been inferred for example in recent scanning tunnelling microscopy [10, 11] and ARPES [20] experiments.

An intriguing pattern emerges upon comparing our results with those on other hole doped cuprate families near p_c . In contrast with Bi-2212 and $\text{La}_{1.6-x}\text{Nd}_{0.4}\text{Sr}_x\text{CuO}_4$ [13] where p_c is located well inside the superconduct-

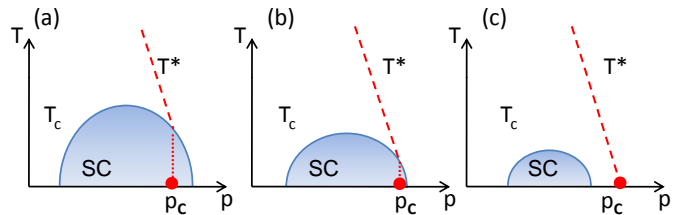


FIG. 5: (Color online) Schematic temperature (T) versus doping p phase diagram with three material-dependent possible locations of the critical doping p_c , where the normal state pseudogap closes, with respect to the superconducting (SC) dome (shaded blue/grey). (a) is realized in Bi-2212 (current study), (b) and (c) have been reported for LSCO [50] and Bi-2201 [51] respectively. The common feature in all three cases is the coincidence of p_c with a Lifshitz transition where a Fermi surface changes from hole-like to electron-like.

ing dome, in ARPES measurements on $\text{La}_{2-x}\text{Sr}_x\text{CuO}_4$ (LSCO) of Ref. [50] the endpoints of the pseudogap and the superconducting phases are nearby in doping. Scanning tunneling spectroscopy on $\text{Bi}_2\text{Sr}_2\text{CuO}_{6+\delta}$ (Bi-2201) instead, found the pseudogap extending well into the normal phase [51]. This suggests that the position of p_c with respect to the superconducting dome is material dependent (see Fig. 5). Interestingly, just as we established here for Bi-2212, for both LSCO and Bi-2201 data analyses have suggested the coincidence of the pseudogap closing with a Lifshitz transition [50, 51]. Taken together, this appears to be a universal feature of the hole doped cuprates, and our findings establish an intimate connection between the normal state pseudogap and Fermi surface topology. In $\text{Tl}_2\text{Ba}_2\text{CuO}_{6+\delta}$ (Tl-2201) the scenario is less clear, as the observation of the pseudogap is still debated [52].

Few studies [16, 53] on Bi-2212 and $\text{YBa}_2\text{Cu}_3\text{O}_{7-x}$ (Y-123) have reported the pseudogap closing at $p = 0.19$. This might simply imply that the normal state and the superconducting pseudogaps close at different dopings [20]. Alternately, this apparent discrepancy could be related to the fact that in-plane transport and superfluid density are mostly sensitive to the nodal properties [37], while c -axis transport and B_{1g} Raman probe mostly the antinodal properties [54]. Next, in our scenario it is possible that for $p > 0.22$ the pseudogap exists in the hole-like B band, but we do not find any signature of it in the Raman spectra, consistently with ARPES results [20]. One possibility is that the response is predominantly from the AB band since it is close to a density of states singularity. We notice this trend in the theoretical calculation as well (cf. SM).

In conclusion, our results demonstrate that the mechanism that gives rise to the normal state pseudogap is sensitive to the topology of the Fermi surface, and is operational only when the latter is hole-like. Furthermore, we conclude that, on the overdoped side of the cuprates,

the microscopic origins of the pseudogap and the superconductivity are different.

We are grateful to A. Georges, J. Tallon, A. Chubukov, M. Norman, L. Taillefer, C. Pépin, Ph. Bourges, Y. Sidis and A. Damascelli for very helpful discussions. Correspondences and requests for materials should be addressed to A.S (alain.sacuto@univ-paris-diderot.fr)

SUPPLEMENTAL MATERIAL

A. Raman Experiments

Raman experiments have been carried out using a triple grating spectrometer (JY-T64000) equipped with a liquid-nitrogen-cooled CCD detector. Two laser excitation lines were used: 532 nm and 647.1 nm from respectively a diode pump solid state laser and a Ar+/Kr+ mixed laser gas. The B_{1g} and B_{2g} geometries were obtained from cross polarizations at 45° from the Cu-O bond directions and along them respectively. The change from B_{1g} to B_{2g} geometries was obtained by keeping fixed the orientations of the analyzers and the polarizers and by rotating the crystal using an Attocube piezo-driven rotator. We got an accuracy on the crystallographic axes orientation with respect to the polarizers close to 2° . Importantly, we succeeded in measuring the B_{1g} and B_{2g} Raman responses of each crystal on the same laser spot. This allowed us to keep constant the solid angle of collection and made reliable the B_{1g} to B_{2g} Raman integrated intensity ratio. Studying the intensity ratio rather than the absolute intensities of the Raman response prevent us from some non intrinsic intensity modulations when passing from one crystal to another.

All the spectra have been corrected for the Bose factor and the instrumental spectral response. They are thus proportional to the imaginary part of the Raman response function $\chi''_{\nu}(\omega)$. Measurements between 4 K and 300 K have been performed using an ARS closed-cycle He cryostat. The laser power at the entrance of the cryostat was maintained below 2 mW to avoid over heating of the crystal estimated to 3 K/mW at 10 K.

B. Crystal Growth and Characterization

The Bi-2212 single crystals were grown by using a floating zone method. The optimal doped sample with $T_c = 90$ K was grown at a velocity of 0.2 mm per hour in air [55]. In order to get overdoped samples down to $T_c = 65$ K, the as-grown single crystal was put into a high oxygen pressured cell between 1000 and 2000 bars and then was annealed from 350°C to 500°C during 3 days [56]. The overdoped samples below $T_c = 60$ K was obtained from as-grown Bi-2212 single crystals put into a pressure cell (Autoclave France) with 100 bars oxygen pressure and annealed from 9 to 12 days at 350°C . Then

the samples were rapidly cooled down to room temperature by maintaining a pressure of 100 bars. The critical temperature T_c for each crystal has been determined from magnetization susceptibility measurements at a 10 Gauss field parallel to the c-axis of the crystal. More than 30 crystals have been measured among 60 tested. The selected crystals exhibit a quality factor of $T_c/\Delta T_c$ larger than 7. ΔT_c is the full width of the superconducting transition. A complementary estimate of T_c was achieved from electronic Raman scattering measurements by defining the temperature from which the B_{1g} superconducting pair breaking peak collapses.

C. Estimate of Δ_0 and its relationship to T_c

The determination of Δ_0 was achieved by subtracting the normal B_{1g} Raman response at 110 K from the B_{1g} one in the superconducting state at 10 K. We define $2\Delta_0$ as the maximum of the electronic background in the subtracted spectra, see Fig.1.

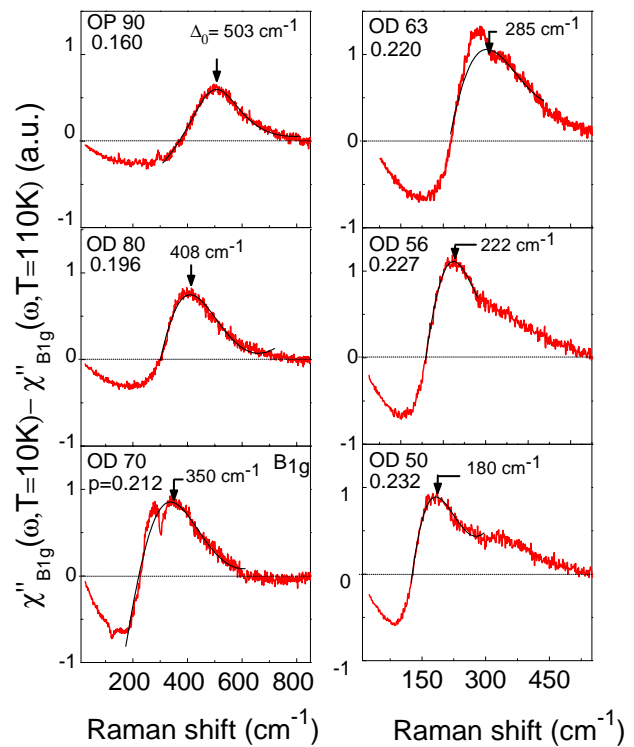


FIG. 6: Subtraction between the normal and superconducting B_{1g} Raman responses of Bi-2212 for several doping levels. The arrows indicate the location of $2\Delta_0$ in wavenumbers. An independent accurate estimate of $2\Delta_0$ for OD 70 and OD 63 compounds was obtained using the 647.1 nm laser line (not shown). For this excitation line the phonon peak at 283 cm^{-1} is no more Raman active and it does not hamper anymore the estimate of $2\Delta_0$.

Special care has been devoted to select single crystals which exhibit the same $2\Delta_0$ value in the Raman spectra

measured from distinct laser spots on a freshly cleaved surface. We find that T_c increases linearly with $2\Delta_0$ in the overdoped regime and reaches its maximum value at $T_c^{max} = 90 K$. From a linear fit of the T_c values in a short range between $T_c = 50 K$ and $T_c = 90 K$, we find the reliable relationship: $T_c = (2\Delta_0)/8.2 + 28.6$. In the underdoped regime T_c falls down abruptly as a function of $2\Delta_0$ (see Fig. 7). The level of doping p was defined from T_c using Presland and Tallon's equation[57]: $1 - T_c/T_c^{max} = 82.6(p - 0.16)^2$. In the overdoped regime, estimate of p can be directly determined from $2\Delta_0$ using the above two equations.

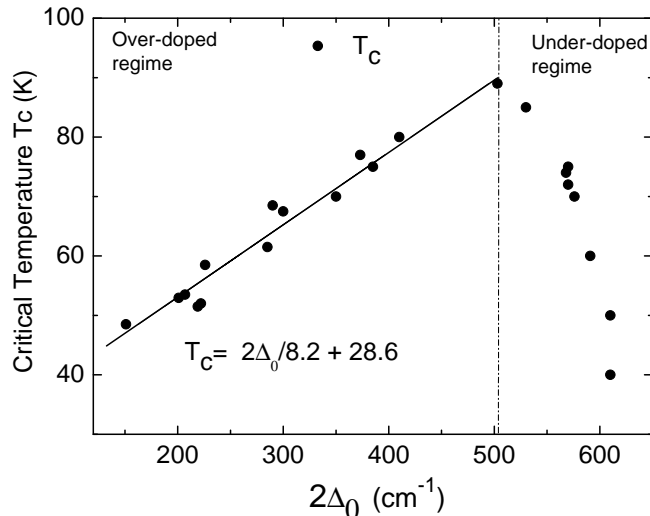


FIG. 7: Evolution of the critical temperature T_c versus pair breaking peak $2\Delta_0$. T_c and $2\Delta_0$ are respectively deduced from magnetic susceptibility and Raman measurements of Bi-2212 crystals with distinct oxygen annealing treatments (see text). The black solid line corresponds to the linear fit of T_c in a restricted range of the overdoped side. The dashed-dotted line marks off the end of the overdoped regime. The maximum value of T_c is reached for $90 K$ which corresponds to $2\Delta_0 = 503 cm^{-1}$.

D. Signature of the pseudogap from B_{1g} integrated Raman Intensity

In Fig.8 is reported the temperature dependence of the B_{1g} Raman response and its integrated Raman intensity for several doping levels. Below $p = 0.22$ the Raman integrated intensity curves exhibit a dip at T_c and reaches a maximum at T_* that defines the onset of the pseudogap. The loss of spectral intensity $I_{B_{1g}}(T_c) - I_{B_{1g}}(T_*)$ is taken as the strength of the pseudogap. For $p=0.11$ (UD 75 crystal, Fig. 8, first row) the strength of the pseudogap is clearly detected and represents 15% of the integrated Raman intensity at $T = 10K$. Importantly, the signature of the pseudogap manifests itself by a positive slope of $I_{B_{1g}}(T)$ just above T_c . This slope stays positive for $p \leq 0.22$, and changes sign only above $p_c = 0.22$. This change of sign has been underlined by fitting $I_{B_{1g}}(T)$ with a

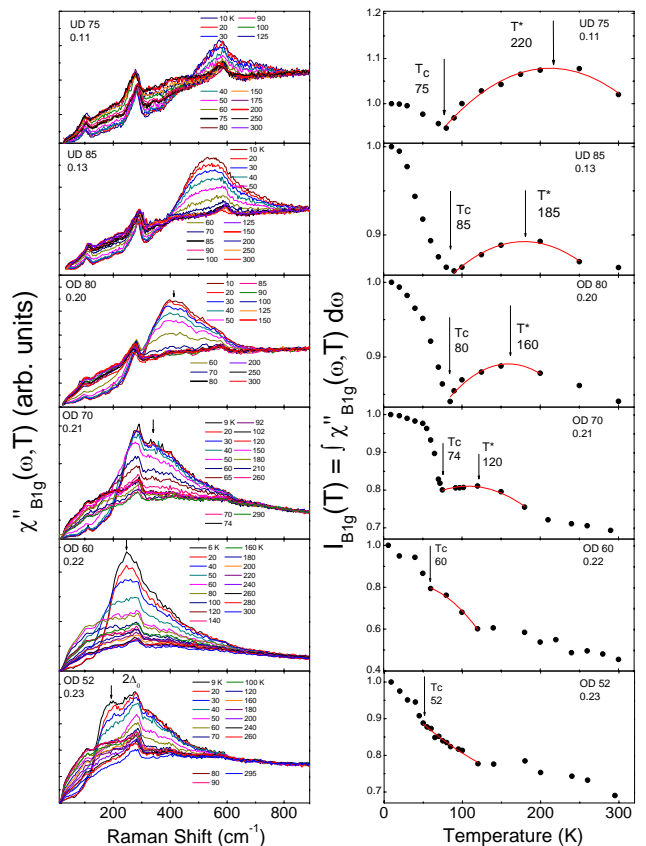


FIG. 8: Temperature dependence of the Raman response $\chi''_{B_{1g}}$ and its integrated Raman intensity $I_{B_{1g}}(T)$ for underdoped and overdoped Bi 2212 single crystals. For each doping level, $I_{B_{1g}}(T)$ has been normalized to this value at $T = 10 K$. Note that for $p=0.11$ (UD 75 crystal) the pseudogap signal is large and represents 15% of the integrated Raman intensity at $T = 10K$. Consequently its doping dependence can be easily tracked.

second order polynomial function (red curve in Fig.8) just above T_c . The absence of the pseudogap is then characterized by a negative slope of $I_{B_{1g}}(T)$ just after T_c .

E. Comparison between T^* determined from Raman and c-axis transport and other spectroscopy probes

It is important to point out that the doping evolution of T^* from our Raman results on Bi-2212 is in good agreement with angle resolved photoemission (ARPES), recent neutron scattering, tunneling and resistivity measurements along the c-axis. This is displayed in Fig.9 and show that the electronic Raman scattering is a reliable probe for detecting the pseudogap and for studying its doping evolution. Note that T^* got from B_{1g} Raman response has been compared to the c-axis tunneling and transport measurements because all these experiments probe mostly the anti-nodal properties (cf. O. K. Anderson, J. Phys. Chem. Sol. **56**, 1573, 1995).

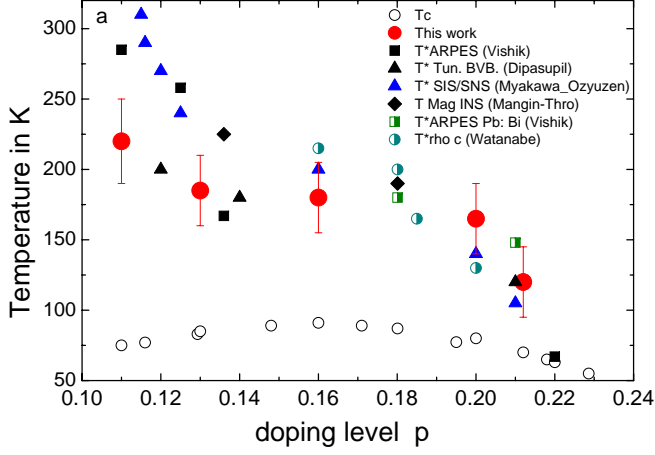


FIG. 9: Comparison between T^* determined by Raman (filled red circles) and transport and other spectroscopic probes. At $p_c = 0.22$ there is no signature of normal state pseudogap (see Fig. 8), consequently $T^*(p_c) = T_c(p_c)$. The references are (i) tunneling : R. M. Disapupil et al. J. Phys. Soc. Jpn. **71**, 1535, (2002), L. Ozyuzer et al., Eur. Phys. Lett. **58**, 589, (2002), N. Miyakawa et al., Phys. Rev. Lett. **83**, 1018, (1999). (ii) resistivity : T. Watanabe et al., Phys. Rev. Lett. **84**, 5848, (2000); T. Usui et al. arXiv:1404.473, (iii) ARPES: I.M. Vishik et al., Proc. Natl. Acad. Sci. **109**, 18332, (2012). (iv) neutron scattering: L.Mangin-Thro et al., Phys. Rev. B **89**, 094523, (2014).

F. Theoretical Raman calculation

We calculate the electronic Raman response using standard zero-temperature linear response theory [58, 59]. This is given by

$$\chi''_{\nu}(\Omega) = \sum_{\alpha=AB,B} \int_{-\Omega}^0 \sum_k (\gamma_{k,\alpha}^{\nu})^2 [\text{Im}G_{\alpha}(k, \omega) \times \text{Im}G_{\alpha}(k, \omega + \Omega) - \text{Im}F_{\alpha}(k, \omega)\text{Im}F_{\alpha}(k, \omega + \Omega)], \quad (2)$$

where the Raman vertex in the geometry $\nu = (B_{1g}, B_{2g})$ is $\gamma_{k,\alpha}^{\nu} = \frac{m}{\hbar^2} \sum_{a,b} e_{a,\nu}^{I,\nu} \frac{\partial^2 \epsilon_k^{\alpha}}{\partial k_a \partial k_b} e_b^{S,\nu}$, with (a, b) denoting spatial directions (x, y) , e^I and e^S are polarization vectors for the incident and the scattered light respectively. The normal-state one particle propagator is given by $G(k, \omega) = 1/(\omega - \epsilon_k + i\Gamma_N)$, while in the superconducting state it can be written in a Nambu formalism:

$$\hat{G}(k, \omega) = \begin{pmatrix} G(k, \omega) & F(k, \omega) \\ F(k, \omega) & -G^*(k, -\omega) \end{pmatrix} = \begin{pmatrix} \omega - \epsilon_k + i\Gamma_S & \Delta_k \\ \Delta_k & \omega + \epsilon_k + i\Gamma_S \end{pmatrix}^{-1} \quad (3)$$

Here we have introduced constant scattering rates $\Gamma_N = 0.01t$ and $\Gamma_S = 0.0025t$ in the normal and superconducting states respectively.

The superconducting gap is given by $\Delta_k = (\Delta_0/2)(\cos k_x - \cos k_y)$, with $\Delta_0 = 0.025t$. Since our

aim is to study only the effect of the Fermi surface topology change and the associated van Hove singularity on the Raman response, we do not change Δ_0 with doping.

The Lifshitz transition in the AB band at the critical doping $p_c = 0.22$ is clearly visible in the B_{1g} Raman response, since in this geometry one probes mainly the antinodal parts of the Fermi surface close to the $k = (0, \pm\pi)$ and $(\pm\pi, 0)$. The Raman-vertex-weighted density of states $N_{B_{1g}}(\omega)$ (defined in the main text) presents in this case a singularity at the chemical potential (see Fig. 3(f), main text), and therefore the $\chi''_{B_{1g}}(\omega)$ increases substantially and present a maximum at p_c , see top panels of Fig. 10 (a) and (b). Instead, the $N_{B_{2g}}(\omega)$ does not present any singularity, since in this geometry one probes mainly the nodal regions of the Brillouin zone. Consequently the B_{2g} Raman response is not affected by the Lifshitz transition, and it displays little doping dependence.

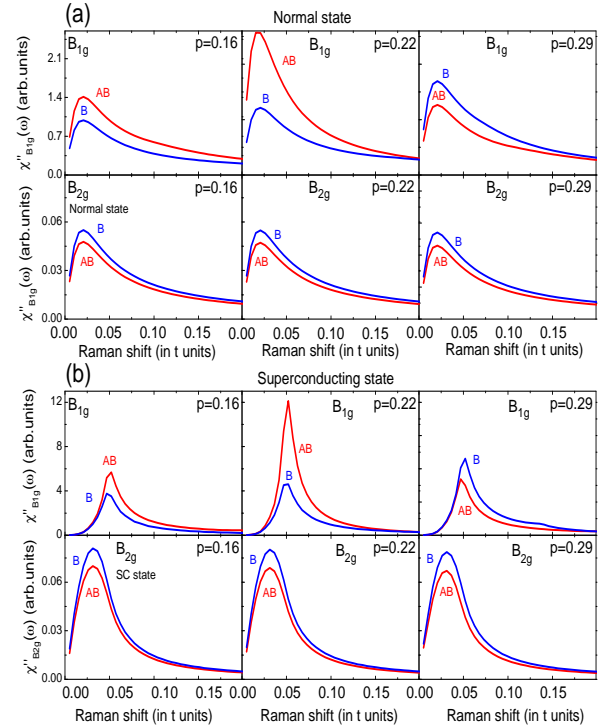


FIG. 10: Raman response evolution (a) in the normal state and (b) superconducting state for three characteristic dopings. The doping level $p = 0.22$ corresponds to a Lifshitz transition where the hole-like AB band becomes electron-like. The AB band contribution is represented by (red/light gray) lines and the B band contribution by (blue/dark gray) lines. Both in the normal and the superconducting states the B_{1g} response of the AB band shows a substantial enhancement at the van Hove singularity associated with its Lifshitz transition. The B_{2g} response, by contrast, is only weakly doping dependent.

In this doping range the B band is far from its own Lif-

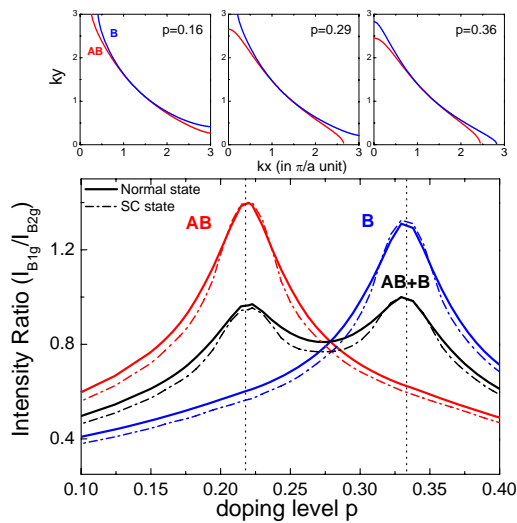


FIG. 11: Integrated intensity ratios $I_{B_{1g}}/I_{B_{2g}}$ for the normal (solid lines) and superconducting (dash-dot lines) phases over a doping range wider than what is accessible experimentally. The contributions from the AB (red/light gray) and B (blue/dark gray) bands are shown separately. They peak at $p = 0.22$ and 0.33 respectively, which correspond to the Lifshitz transitions in each of these bands, as shown in the top panel. Note that around $p = 0.22$ the AB band contribution is dominant. The physical intensity ratios obtained from the total responses, i.e., the sum of the responses from the two bands, is shown in black. All the curves for a given phase are normalized by the value of the total response in that phase at $p = 0.22$.

shitz transition, which would take place at a much higher doping $p = 0.33$ which is inaccessible experimentally. Therefore, its contribution to the Raman B_{1g} response (blue/ dark gray) curves in Fig. 10) is less relevant than the AB band one (red/light gray) around $p = 0.22$.

For the sake of completeness in Fig. 11 we show the calculated ratio of the total integrated Raman intensities $I_{B_{1g}}/I_{B_{2g}}$ (defined in main text) for a doping range larger than what is accessible experimentally. Two peaks are clearly discernable, both in the normal and the superconducting cases, at $p = 0.22$ and at $p = 0.33$, the first corresponding to the AB band Lifshitz transition, the second to that of the B band.

For clarity we also plot the $I_{B_{1g}}/I_{B_{2g}}$ for the AB and B bands separately, which shows that the contribution of each band peaks at its respective Lifshitz transition point.

In particular, as we previously stated, the B band contribution to the Raman response at $p = 0.22$ doping is substantially smaller than the AB band one (while the converse is true at $p = 0.33$). We also display in the top panels of Fig. 11 the Fermi surface in the first quadrant of the Brillouin zone. We clearly observe the change of topology from an hole- to electron-like Fermi surface in the AB and B bands, for $p = 0.22$ and for $p = 0.33$

respectively.

- [1] H. Alloul, T. Ohno, and P. Mendels, *Phys. Rev. Lett.* **63**, 1700 (1989), URL <http://link.aps.org/doi/10.1103/PhysRevLett.63.1700>.
- [2] W. W. Warren, R. E. Walstedt, G. F. Brennert, R. J. Cava, R. Tycko, R. F. Bell, and G. Dabbagh, *Phys. Rev. Lett.* **62**, 1193 (1989), URL <http://link.aps.org/doi/10.1103/PhysRevLett.62.1193>.
- [3] T. Imai, H. Yasuoka, T. Shimizu, Y. Ueda, K. Yoshimura, and K. Kosuge, *Physica C: Superconductivity* **162164**, Part 1, 169 (1989), ISSN 0921-4534, URL <http://www.sciencedirect.com/science/article/pii/S0921453489909714>.
- [4] T. Timusk and B. Statt, *Reports on Progress in Physics* **62**, 61 (1999), URL <http://stacks.iop.org/0034-4885/62/i=1/a=002>.
- [5] M. R. Norman, D. Pines, and C. Kallin, *Advances in Physics* **54**, 715 (2005).
- [6] L. Taillefer, *Annual Review of Condensed Matter Physics* **1**, 51 (2010), URL <http://dx.doi.org/10.1146/annurev-conmatphys-070909-104117>.
- [7] J. Loram, J. Luo, J. Cooper, W. Liang, and J. Tallon, *Journal of Physics and Chemistry of Solids* **62**, 59 (2001), ISSN 0022-3697, URL <http://www.sciencedirect.com/science/article/pii/S0022369700001013>.
- [8] A. Shekhter, B. J. Ramshaw, L. R. H. W. N., B. D. A., B. F. F., R. D. McDonald, B. J. B., R. S. C., and M. A., *Nature* **498**, 75 (2013), ISSN 0028-0836, URL <http://dx.doi.org/10.1038/nature12165>.
- [9] L. Mangin-Thro, Y. Sidis, P. Bourges, S. De Almeida-Didry, F. Giovannelli, and I. Laffez-Monot, *Phys. Rev. B* **89**, 094523 (2014), URL <http://link.aps.org/doi/10.1103/PhysRevB.89.094523>.
- [10] K. Fujita, C. K. Kim, I. Lee, J. Lee, M. H. Hamidian, I. A. Firmo, S. Mukhopadhyay, H. Eisaki, S. Uchida, M. J. Lawler, et al., *Science* **344**, 612 (2014), URL <http://www.sciencemag.org/content/344/6184/612.abstract>.
- [11] Y. He, Y. Yin, M. Zech, A. Soumyanarayanan, M. M. Yee, T. Williams, M. C. Boyer, K. Chatterjee, W. D. Wise, I. Zeljkovic, et al., *Science* **344**, 608 (2014).
- [12] Y. H. Liu, Y. Toda, K. Shimatake, N. Momono, M. Oda, and M. Ido, *Phys. Rev. Lett.* **101**, 137003 (2008), URL <http://link.aps.org/doi/10.1103/PhysRevLett.101.137003>.
- [13] R. Daou, N. Doiron-Leyraud, D. LeBoeuf, S. Y. Li, F. Laliberte, O. Cyr-Choiniere, Y. J. Jo, L. Balicas, J.-Q. Yan, J.-S. Zhou, et al., *Nat Phys* **5**, 31 (2009), ISSN 1745-2473, URL <http://dx.doi.org/10.1038/nphys1109>.
- [14] H. Alloul, J. Bobroff, M. Gabay, and P. J. Hirschfeld, *Rev. Mod. Phys.* **81**, 45 (2009), URL <http://link.aps.org/doi/10.1103/RevModPhys.81.45>.
- [15] C. M. Varma, *Phys. Rev. Lett.* **83**, 3538 (1999), URL <http://link.aps.org/doi/10.1103/PhysRevLett.83.3538>.
- [16] J. Tallon and J. Loram, *Physica C: Superconductivity* **349**, 53 (2001), ISSN 0921-4534, URL <http://www.sciencedirect.com/science/article/pii/S0921453400015240>.
- [17] S. Sachdev, *Physica C: Superconductivity* **470**, Supplement 1, S4 (2010), ISSN 0921-4534, proceedings of the 9th International Conference on Materials and Mechanisms of Superconductivity, URL <http://www.sciencedirect.com/science/article/pii/S0921453409007205>.
- [18] A. Sacuto, Y. Gallais, M. Cazayous, M.-A. Méasson, G. D. Gu, and D. Colson, *Reports on Progress in Physics* **76**, 022502 (2013), URL <http://stacks.iop.org/0034-4885/76/i=2/a=022502>.
- [19] U. Chatterjee, D. Ai, J. Zhao, S. Rosenkranz, A. Kaminski, H. Raffy, Z. Li, K. Kadowaki, M. Randeria, M. R. Norman, et al., *Proceedings of the National Academy of Sciences* **108**, 9346 (2011), URL <http://www.pnas.org/content/108/23/9346.abstract>.
- [20] I. M. Vishik, M. Hashimoto, R.-H. He, W.-S. Lee, F. Schmitt, D. Lu, R. G. Moore, C. Zhang, W. Meevasana, T. Sasagawa, et al., *Proceedings of the National Academy of Sciences* **109**, 18332 (2012), URL <http://www.pnas.org/content/109/45/18332.abstract>.
- [21] A. Kaminski, S. Rosenkranz, H. M. Fretwell, M. R. Norman, M. Randeria, J. C. Campuzano, J.-M. Park, Z. Z. Li, and H. Raffy, *Phys. Rev. B* **73**, 174511 (2006), URL <http://link.aps.org/doi/10.1103/PhysRevB.73.174511>.
- [22] F. Venturini, M. Opel, T. P. Devereaux, J. K. Freericks, I. Tütto, B. Revaz, E. Walker, H. Berger, L. Forró, and R. Hackl, *Phys. Rev. Lett.* **89**, 107003 (2002), URL <http://link.aps.org/doi/10.1103/PhysRevLett.89.107003>.
- [23] F. Venturini, M. Opel, R. Hackl, L. Berger, H. and Forró, and B. Revaz, *J. of Phys. Chem. of Solids* **63**, 2345 (2002).
- [24] S. Blanc, Y. Gallais, A. Sacuto, M. Cazayous, M. A. Méasson, G. D. Gu, J. S. Wen, and Z. J. Xu, *Phys. Rev. B* **80**, 140502 (2009), URL <http://link.aps.org/doi/10.1103/PhysRevB.80.140502>.
- [25] K. C. Hewitt and J. C. Irwin, *Phys. Rev. B* **66**, 054516 (2002), URL <http://link.aps.org/doi/10.1103/PhysRevB.66.054516>.
- [26] N. Munnikes, B. Muschler, F. Venturini, L. Tassini, W. Prestel, S. Ono, Y. Ando, D. C. Peets, W. N. Hardy, R. Liang, et al., *Phys. Rev. B* **84**, 144523 (2011), URL <http://link.aps.org/doi/10.1103/PhysRevB.84.144523>.
- [27] T. Masui, M. Limonov, H. Uchiyama, S. Lee, S. Tajima, and A. Yamanaka, *Phys. Rev. B* **68**, 060506 (2003), URL <http://link.aps.org/doi/10.1103/PhysRevB.68.060506>.
- [28] T. Masui, T. Hiramachi, K. Nagasao, and S. Tajima, *Phys. Rev. B* **79**, 014511 (2009), URL <http://link.aps.org/doi/10.1103/PhysRevB.79.014511>.
- [29] J. G. Naeni, X. K. Chen, J. C. Irwin, M. Okuya, T. Kimura, and K. Kishio, *Phys. Rev. B* **59**, 9642 (1999), URL <http://link.aps.org/doi/10.1103/PhysRevB.59.9642>.
- [30] L. V. Gasparov, P. Lemmens, N. N. Kolesnikov, and G. Güntherodt, *Phys. Rev. B* **58**, 11753 (1998), URL <http://link.aps.org/doi/10.1103/PhysRevB.58.11753>.
- [31] The phonon peak contribution is less than 3% of the total integrated area.
- [32] A. A. Kordyuk, S. V. Borisenko, M. Knupfer, and J. Fink,

- Phys. Rev. B **67**, 064504 (2003), URL <http://link.aps.org/doi/10.1103/PhysRevB.67.064504>.
- [33] J. M. Buhmann and M. Sigrist, Phys. Rev. B **88**, 115128 (2013), URL <http://link.aps.org/doi/10.1103/PhysRevB.88.115128>.
- [34] Z. Konstantinović, Z. Z. Li, and H. Raffy, Phys. Rev. B **62**, R11989 (2000), URL <http://link.aps.org/doi/10.1103/PhysRevB.62.R11989>.
- [35] A. V. Chubukov, EPL (Europhysics Letters) **44**, 655 (1998), URL <http://stacks.iop.org/0295-5075/44/i=5/a=655>.
- [36] J. Schmalian, D. Pines, and B. Stojković, Phys. Rev. Lett. **80**, 3839 (1998), URL <http://link.aps.org/doi/10.1103/PhysRevLett.80.3839>.
- [37] L. B. Ioffe and A. J. Millis, Phys. Rev. B **58**, 11631 (1998), URL <http://link.aps.org/doi/10.1103/PhysRevB.58.11631>.
- [38] S. Chakravarty, R. B. Laughlin, D. K. Morr, and C. Nayak, Phys. Rev. B **63**, 094503 (2001), URL <http://link.aps.org/doi/10.1103/PhysRevB.63.094503>.
- [39] Y. Wang and A. Chubukov, Phys. Rev. B **90**, 035149 (2014), URL <http://link.aps.org/doi/10.1103/PhysRevB.90.035149>.
- [40] R. Comin, A. Frano, M. M. Yee, Y. Yoshida, H. Eisaki, E. Schierle, E. Weschke, R. Sutarto, F. He, A. Soumyanarayanan, et al., Science **343**, 390 (2014), URL <http://www.sciencemag.org/content/343/6169/390.abstract>.
- [41] E. H. da Silva Neto, P. Aynajian, A. Frano, R. Comin, E. Schierle, E. Weschke, A. Gyenis, J. Wen, J. Schneeloch, Z. Xu, et al., Science **343**, 393 (2014), URL <http://www.sciencemag.org/content/343/6169/393.abstract>.
- [42] T. Wu, H. Mayaffre, S. Krämer, M. Horvatić, C. Berthier, W. N. Hardy, R. Liang, D. A. Bonn, and M.-H. Julien (2014), 1404.1617.
- [43] S. E. Sebastian, N. Harrison, F. F. Balakirev, M. M. Altarawneh, P. A. Goddard, R. Liang, D. A. Bonn, W. N. Hardy, and G. G. Lonzarich, Nature **511**, 61 (2014), ISSN 0028-0836, URL <http://dx.doi.org/10.1038/nature13326>.
- [44] C. Pépin, V. S. de Carvalho, T. Kloss, and X. Montiel (2014), 1408.5908.
- [45] M. Civelli, M. Capone, S. S. Kancharla, O. Parcollet, and G. Kotliar, Phys. Rev. Lett. **95**, 106402 (2005), URL <http://link.aps.org/doi/10.1103/PhysRevLett.95.106402>.
- [46] B. Kyung, S. S. Kancharla, D. Sénéchal, A.-M. S. Tremblay, M. Civelli, and G. Kotliar, Phys. Rev. B **73**, 165114 (2006), URL <http://link.aps.org/doi/10.1103/PhysRevB.73.165114>.
- [47] M. Ferrero, P. S. Cornaglia, L. De Leo, O. Parcollet, G. Kotliar, and A. Georges, Phys. Rev. B **80**, 064501 (2009), URL <http://link.aps.org/doi/10.1103/PhysRevB.80.064501>.
- [48] S. Sakai, S. Blanc, M. Civelli, Y. Gallais, M. Cazayous, M.-A. Méasson, J. S. Wen, Z. J. Xu, G. D. Gu, G. Sangiovanni, et al., Phys. Rev. Lett. **111**, 107001 (2013), URL <http://link.aps.org/doi/10.1103/PhysRevLett.111.107001>.
- [49] G. Sordi, K. Haule, and A.-M. S. Tremblay, Phys. Rev. B **84**, 075161 (2011), URL <http://link.aps.org/doi/10.1103/PhysRevB.84.075161>.
- [50] A. Ino, C. Kim, M. Nakamura, T. Yoshida, T. Mizokawa, A. Fujimori, Z.-X. Shen, T. Kakeshita, H. Eisaki, and S. Uchida, Phys. Rev. B **65**, 094504 (2002), URL <http://link.aps.org/doi/10.1103/PhysRevB.65.094504>.
- [51] A. Piriou, N. Jenkins, C. Berthod, I. Maggio-Aprile, and O. Fischer, Nat Commun **2**, 221 (2011), URL <http://dx.doi.org/10.1038/ncomms1229>.
- [52] D. C. Peets, J. D. F. Mottershead, B. Wu, I. S. Elfimov, R. Liang, W. N. Hardy, D. A. Bonn, M. Raudsepp, N. J. C. Ingle, and A. Damascelli, New Journal of Physics **9**, 28 (2007).
- [53] Y. Ando, S. Komiya, K. Segawa, S. Ono, and Y. Kurita, Phys. Rev. Lett. **93**, 267001 (2004), URL <http://link.aps.org/doi/10.1103/PhysRevLett.93.267001>.
- [54] O. Andersen, A. Liechtenstein, O. Jepsen, and F. Paulsen, Journal of Physics and Chemistry of Solids **56**, 1573 (1995), ISSN 0022-3697, proceedings of the Conference on Spectroscopies in Novel Superconductors, URL <http://www.sciencedirect.com/science/article/pii/S0022369795002693>.
- [55] J. Wen, Z. Xu, G. Xu, M. Hcker, J. Tranquada, and G. Gu, Journal of Crystal Growth **310**, 1401 (2008), ISSN 0022-0248, the Proceedings of the 15th International Conference on Crystal Growth (ICCG-15) in conjunction with the International Conference on Vapor Growth and Epitaxy and the {US} Biennial Workshop on Organometallic Vapor Phase Epitaxy, URL <http://www.sciencedirect.com/science/article/pii/S0022024807007865>.
- [56] L. Mihaly, C. Kendziora, J. Hartge, D. Mandrus, and L. Forro, Review of Scientific Instruments **64**, 2397 (1993), URL <http://scitation.aip.org/content/aip/journal/rsi/64/8/10.1063/1.1144459>.
- [57] M. Presland, J. Tallon, R. Buckley, R. Liu, and N. Flower, Physica C: Superconductivity **176**, 95 (1991), ISSN 0921-4534, URL <http://www.sciencedirect.com/science/article/pii/0921453491907009>.
- [58] T. P. Devereaux and R. Hackl, Rev. Mod. Phys. **79**, 175 (2007), URL <http://link.aps.org/doi/10.1103/RevModPhys.79.175>.
- [59] A. V. Chubukov and M. R. Norman, Phys. Rev. B **77**, 214529 (2008), URL <http://link.aps.org/doi/10.1103/PhysRevB.77.214529>.